^{6}Li and ^{7}Li MAS NMR Studies of Lithium Manganate Cathode Materials

Young Joo Lee, Francis Wang, and Clare P. Grey*

Contribution from the Department of Chemistry, State University of New York at Stony Brook, Stony Brook, New York 11794-3400

Received May 21, 1998. Revised Manuscript Received October 16, 1998

Abstract: ^{6}Li MAS NMR has been used to study the lithium local environments and manganese electronic structures of a number of lithium manganese oxides with manganese oxidation states varying from (III) to (IV). Most samples were chosen with compositions within the $LiMn_2O_4-Li_2Mn_4O_9-Li_4Mn_5O_{12}$ phase diagram, but $Li_2Mn_2O_4$ with Mn(III) was also synthesized for comparison. Despite the presence of unpaired electrons, high-resolution spectra could still be acquired, allowing a number of different local environments to be detected. Assignments of the resonances to different lithium local environments were made by comparing the observed shifts and local structures in a number of lithium manganates. Two ^{6}Li NMR resonances were observed for the spinel phase $Li_4Mn_5O_{12}$ at 1980 and 847 ppm, which were assigned to Li^+ in the octahedral and tetrahedral sites of the spinel structure, respectively. A shift was observed for Li^+ in the tetrahedral site of $Li_2Mn_4O_9$, which also contains Mn(IV), at 687 ppm. The shifts are ascribed primarily to a Fermi-contact shift mechanism, and possible mechanisms to account for the directions and sizes of the shift are discussed. Shifts to lower frequency are observed as the manganese oxidation state is reduced (i.e., for manganates containing occupied e_g orbitals). The ^{6}Li MAS NMR spectra of the spinels with a Li:Mn ratio of 1:2 are extremely sensitive to the synthesis conditions. When relatively high synthesis temperatures (850 °C) are used, a single resonance at 520 ppm, from the normal spinel phase, dominates. In contrast, several resonances are observed for samples synthesized at lower temperatures (550−650 °C), as a result of defects in the normal spinel structure. These resonances collapse into the main spinel resonance at high temperatures (250 °C) and are assigned to electronic defects associated with higher oxidation state manganese ions (Mn^{4+}). No evidence for a Jahn−Teller distortion is observed in both the NMR and by diffraction for samples that contain considerable disorder. In contrast, samples that were prepared at temperatures of 650 °C or higher show a cubic-to-tetragonal phase change below room temperature. This is accompanied by the appearance of at least three additional ^{6}Li resonances, indicating some ordering of the Mn^{3+} and Mn^{4+} cations below the phase transition, in the time scale of the NMR experiment.

Introduction

Lithium intercalation materials have been widely studied with a view to developing new electrode materials for compact, high-voltage rechargeable batteries.[1] The first commercial success with this technology was the cathode material $LiCoO_2$, introduced by SONY Energytec in 1990.[2] The SONY cell consists of $LiCoO_2$ and powdered graphite as the cathode and anode, respectively. During the charging and discharging process, Li^+ ions are shuttled between two intercalation hosts. The high cost and toxicity of cobalt has resulted in the search for cheaper and more environmentally friendly alternatives. Lithium manganese oxides $Li_xMn_2O_4$ are promising intercalation cathode materials, meeting cost, toxicity, and efficiency criteria. Problems still remain in the reproducible production of these materials. In addition, structural changes can occur during the charging and discharging processes, which may affect both short-term and long-term behavior of the material within the battery.[1,3]

In this paper, we present the results from a ^{6}Li and ^{7}Li MAS NMR study of a series of lithium manganese oxides. MAS NMR was chosen to study these materials, since it is ideally suited to study local structure and disorder in these materials. The effect of synthesis conditions and of various lithium local environments on the ^{6}Li MAS NMR is explored. Results from the discharging and charging of cells constructed with the lithium manganese materials will be presented in a subsequent paper.

An expanded region of the Li−Mn−O ternary phase diagram is shown in Figure 1.[4] The tie line between Mn_3O_4 and $Li_4Mn_5O_{12}$ represents stoichiometric spinel phases, which can be expressed by the general formula $Li_xMn_{3-x}O_4$ ($0 \le x \le 1.33$). Lithium manganese oxide defect spinels Mn(IV) of general formula $Li_2O{\cdot}yMnO_2$ ($y > 2.5$) are located on the tie line between $Li_4Mn_5O_{12}$ and λ-MnO_2. Manganese oxide defect spinels, $Mn_{3-x}O_4$, ($0 \le x \le 1$), lie between Mn_3O_4 and λ-MnO_2, whereas phases with the rock-salt structure and stoichiometry $Li_zMn_{3-z}O_3$ ($0 \le z \le 2$) are found between MnO and Li_2MnO_3. Regions I and II represent defect spinel and defect rock-salt phases, respectively. The normal spinel structure $A[B_2]X_4$ possesses the crystallographic space group *Fd*3*m*, where the B cations occupy 16d octahedral sites and the A cations occupy

* To whom correspondence should be addressed.

(1) Bruce, P. G. *Chem. Commun.* **1997**, 1817.

(2) Nagaura, T.; Tazawa, K. *Prog. Batteries Sol. Cells* **1990**, *9*, 20.

(3) Gummow, R. J.; De Kock, A.; Thackeray, M. M. *Solid State Ionics* **1994**, *69*, 59.

(4) Thackeray, M. M.; De Kock, A.; Rossouw, M. H.; Liles, D.; Bittihn, R.; Hoge, D. *J. Electrochem. Soc.* **1992**, *139*, 363.

10.1021/ja9817794 CCC: $15.00
Published on Web 11/19/1998

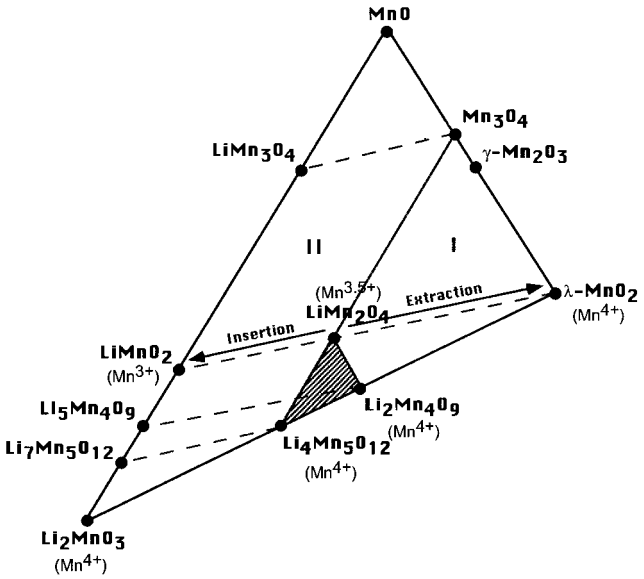

Figure 1. The lithium−manganese−oxygen ternary phase diagram after refs 4 and 13.

8a tetrahedral sites in a cubic close-packed array of X anions.[5,6] There are three additional vacant sites, i.e., the 16c octahedral sites, 8b tetrahedral sites, and 48f tetrahedral sites. The ideal material $LiMn_2O_4$ adopts the normal spinel structure with lithium in the 8a tetrahedral sites and manganese in the 16d octahedral sites. The average manganese oxidation number is +3.5, half the manganese ions having a high spin $3d^4$ ($t_{2g}^3e_g^1$) electronic configuration and the other half existing as Mn^{4+} ions with a $3d^3(t_{2g}^3)$ electronic configuration. The material is a hopping or small polaron semiconductor,[7,8] electronic conduction occurring via hopping of electrons between e_g orbitals on adjacent Mn^{3+}/Mn^{4+} cations. The defect spinel $Li_2Mn_4O_9$, whose formula can be written as $(Li_{0.89}\square_{0.11})_{tet}[Mn_{1.78}\square_{0.22}]_{oct}O_4$ in spinel notation,[4] has been shown, from neutron diffraction studies, to contain vacancies (□) on both of the Li 8a sites and Mn 16d sites.[9] $Li_4Mn_5O_{12}$ is a lithium-rich stoichiometric cubic spinel, in which some of the manganese cations are displaced by lithium cations resulting in the formula: $Li_{tet}[Li_{0.33}Mn_{1.67}]_{oct}O_4$. Both $Li_2Mn_4O_9$ and $Li_4Mn_5O_{12}$ have a manganese oxidation state of +4 and an electronic configuration of $3d^3$ (t_{2g}^3). Lithium can be inserted into or extracted from spinels by electrochemical or chemical redox reactions, (at approximately 3 and 4 V, respectively, versus Li), following the dashed lines in Figure 1.[4] The insertion of lithium into the structure (e.g., during the discharging process) results in the simultaneous displacement of 8a lithium cations onto 16c sites until $Li_2Mn_2O_4$ is formed, which has the tetragonal rock-salt structure (space group $I4_1/amd$).[9,10] Note that an orthorhombic rock-salt structure is formed by direct solid-state reaction. This phase is known as $LiMnO_2$ and crystallizes in the space group *Pmmn*.[11,12] Lithium insertion lowers the average valency of the manganese ions below +3.5, which in turn induces a Jahn−Teller (JT) distortion due to the predominance of JT-active Mn^{3+} (d^4) ions.[5] This results in a cubic-to-tetragonal phase transition, and an increase in the unit cell volume of 6.5%.[3,10] The occurrence of the JT-distortion during cycling of the lithium cells is thought to be one cause of poor cycling behavior.[4] Defect spinels such as $Li_2Mn_4O_9$ and $Li_4Mn_5O_{12}$ have been shown to have improved cyclability in the 2.5−3.5 V range, compared to $LiMn_2O_4$, because the manganese oxidation state is maintained above +3.5 during most of the discharging process, and the cubic-to-tetragonal phase transitions, when they occur, are associated with much smaller changes in cell volumes.[4] Similarly, cyclability at the 4 V plateau may be improved by doping in divalent cations such as Mg^{2+} or Zn^{2+} or by doping in extra Li^+; this prevents the manganese oxidation state from dropping below +3.5 at the end of the (4 V) discharging process.[3]

There have been numerous studies of the $LiMn_2O_4$−$Li_2Mn_4O_9$−$Li_4Mn_5O_{12}$ system which have focused on, for example, the effect of the starting materials, synthesis temperature, Li/Mn ratio, manganese oxidation state, electrochemical properties, occurrence of cubic-to-tetragonal phase transitions, and the magnetic properties.[13−23] The stoichiometry and manganese oxidation state depend on the synthesis temperature: $Li_2Mn_4O_9$ (Mn^{4+}) is formed at 400 °C, and an increase of temperature results in the formation of the defect spinels $Li_{1-\delta}Mn_{2-2\delta}O_4$ ($0 \le \delta \le 0.11$) with a progressive reduction of the manganese oxidation state. Eventually, an average oxidation state for manganese of 3.5 is achieved in the stoichiometric material $LiMn_2O_4$ synthesized at ~850 °C.[13] Li-rich spinels $Li_{1+\delta}Mn_{2-\delta}O_4$ ($0 \le \delta \le 0.33$), with lithium on the manganese 16d sites, are reported to form in preference to the defect spinel for Li/Mn ratios greater than 0.5, under low-temperature synthesis conditions.[13,21−23]

Knowledge concerning the local structure in these materials is crucial to the understanding of their performance as electrodes. Diffraction studies yield long-range structural information but do not directly yield information concerning the local order and environment of the cations. ^{6}Li ($I = 1$) and ^{7}Li ($I = 3/2$) NMR are ideal probes of lithium local environments in these complex systems. ^{7}Li NMR spectra are affected by homonuclear dipolar coupling and the second-order quadrupolar interaction, both of which can give rise to broadening.[24,25] In addition, the satellite transitions, which are broadened by the first-order quadrupolar interaction, can span many kHz. In contrast to ^{7}Li, the much smaller quadrupolar coupling constants typically observed for

(5) Wells, A. F. *Structural Inorganic Chemistry*; Oxford University Press: Oxford, 1993.
(6) West, A. R. *Solid State Chemistry and its Application*; John Wiley & Sons: New York, 1992; Chapter 16.
(7) Tuller, H. L.; Nowick, A. S. *J. Phys. Chem. Solids* **1997**, *38*, 859.
(8) Sugiyama, J.; Atsumi, T.; Koiwai, A.; Sasaki, T.; Hioki, T.; Noda, S.; Kamegashira, N. *J. Phys.: Condens. Matter* **1997**, *9*, 1729.
(9) David, W. I. F.; Thackeray, M. M.; De Picciotto, L. A.; Goodenough, J. B. *J. Solid State Chem.* **1987**, *67*, 316.
(10) Thackeray, M. M.; David, W. I. F.; Bruce, P. G.; Goodenough, J. B. *Mater. Res. Bull.* **1983**, *18*, 461.
(11) Greedan, J. E.; Raju, N. P.; Davidson, I. J. *J. Solid State Chem.* **1997**, *128*, 209.
(12) Gummow, R. J.; Liles, D. C.; Thackeray, M. M. *Mater. Res. Bull.* **1993**, *28*, 1249.
(13) Masquelier, C.; Tabuchi, M.; Ado, K.; Kanno, R.; Kobayashi, Y.; Maki, Y.; Nakamura, O.; Goodenough, J. B. *J. Solid State Chem.* **1996**, *123*, 255.
(14) Barboux, P.; Tarascon, J. M.; Shokoohi, F. K. *J. Solid State Chem.* **1991**, *94*, 185.
(15) Endres, P.; Fuchs, B.; Kemmler-Sack, S.; Brandt, K.; Faust-Becker, G.; Praas, H.-W. *Solid State Ionics* **1996**, *89*, 221.
(16) Rossouw, M. H.; De Kock, A.; De Picciotto, L. A.; Thackeray, M. M. *Mater. Res. Bull.* **1990**, *25*, 173.
(17) Massarotti, V.; Capsoni, D.; Bini. M.; Chiodelli, G.; Azzoni, C. B.; Mozzati, M. C.; Paleari, A. *J. Solid State Chem.* **1997**, *131*, 94.
(18) Shimakawa, Y.; Numata, T.; Tabuchi, J. *J. Solid State Chem.* **1997**, *131*, 138.
(19) Takada, T.; Hayakawa, H.; Akiba, E. *J. Solid State Chem.* **1995**, *115*, 420.
(20) De Kock, A.; Rossouw, M. H.; De Picciotto, L. A.; Thackeray, M. M.; David, W. I. F.; Ibberson, R. M. *Mater. Res. Bull.* **1990**, *25*, 657.
(21) Thackeray, M. M.; De Kock, A.; David, W. I. F. *Mater. Res. Bull.* **1993**, *28*, 1041.
(22) Yamada, A. *J. Solid State Chem.* **1996**, *122*, 160.
(23) Feng, Q.; Miyai, Y.; Kanoh, H.; Ooi, K. *Langmuir* **1992**, *8*, 1861.
(24) Xu, Z.; Stebbins, J. F. *Solid State Nucl. Magn. Reson*. **1995**, *5*, 103.
(25) Eckert, H.; Zhang, Z.; Kennedy, J. H. *Chem. Mater.* **1990**, *2*, 273.

^{6}Li and weaker homonuclear dipolar coupling allow higher resolution spectra to be obtained. The acquisition of high-resolution NMR spectra from the lithium manganese oxide system is further complicated by the paramagnetism of these materials. Large interactions between the nuclear and unpaired electron spins will occur in these systems, which can give rise to broad and sometimes undetectable NMR resonances. Very fast spinning MAS NMR can help remove or reduce interactions, reducing the number of sidebands and simplifying the spectra.[26−28] Spin-echo mapping techniques have also been used in paramagnetic systems to detect extremely broad resonances.[29] A number of ^{6}Li and ^{7}Li NMR experiments have been performed on the $LiCoO_2$ and $LiNi_{1-y}CoO_2$ systems.[30−32] A short paper of the ^{7}Li and ^{6}Li MAS NMR spectra of $LiMn_2O_4$ and Li_2MnO_3 has been published.[33] ^{7}Li MAS NMR of Li−Mn−O and Li−Mn−V−O compounds have also been reported.[34] Large shifts were observed for the ternary spinels, which were ascribed to a Knight-shift mechanism, whereas no significant shifts were observed for the quaternary spinels. Interpretation of the spectra was complicated by the very large spinning sideband manifolds and poor signal-to-noise ratios; hence, accurate shift information could not be readily obtained. An earlier brief paper also interpreted the observed shifts in terms of a Knight-shift mechanism.[35] A more recent paper by Mustarelli et al. of $LiMn_2O_4$ and Li_2MnO_3 and a material with intermediate composition showed, however, that the major source of the large shifts in these compounds is the Fermi-contact shift mechanism.[36] More recent wide-line NMR studies have also interpreted ^{7}Li shifts in terms of a hyperfine or contact interaction.[37] Finally, a number of static ^{7}Li NMR variable-temperature studies have been performed to investigate, in particular, any possible magnetic ordering of the Mn^{3+}/Mn^{4+} ions below the cubic-to-tetragonal phase transition and the Neel temperature.[38]

The aim of the research presented in this paper, was to determine the feasibility of using MAS NMR to study the local order of the lithium cations in lithium manganese oxide systems, and to explore the structural and electronic properties that are responsible for the large shifts observed in these systems. The ^{6}Li MAS NMR of lithium manganese spinels synthesized under a variety of conditions are reported. Spinel phases containing manganese in the +4 oxidation state only have also been synthesized to help rationalize the shifts of both the non- and stoichiometric materials containing manganese in variable oxidation states. $Li_2Mn_2O_4$, which contains Mn^{3+} exclusively, was also synthesized to aid in the interpretation of the NMR data.

Table 1. Temperatures and Reaction Times Used to Prepare the Spinel Samples and the Nomenclature Used to Label the Samples

sample	sample label	starting materials	firing temperature (°C) and time	nominal Li/Mn ratio
$LiMn_2O_4$	LiMn850	Li_2CO_3, Mn_2O_3	650, 12 h and 850, 24 h	1/2
$LiMn_2O_4$	LiMn650	Li_2CO_3, Mn_2O_3	650, 48 h	1/2
$LiMn_2O_4$	LiMn600	Li_2CO_3, Mn_2O_3	600, 48 h	1/2
$LiMn_2O_4$	LiMn550	Li_2CO_3, Mn_2O_3	550, 48 h	1/2
$Li_2Mn_4O_9$	$Li_2Mn_4O_9$	Li_2CO_3, $MnCO_3$	400, 48 h	1/2
$Li_4Mn_5O_{12}$	$Li_4Mn_5O_{12}$	Li_2CO_3, $MnCO_3$	400, 48 h	4/5

Experimental Section

Sample Preparation. $LiMn_2O_4$, $Li_2Mn_4O_9$, and $Li_4Mn_5O_{12}$ were prepared in air by solid-state reaction of lithium and manganese sources. The starting materials were ground together and formed into pellets. The starting materials and firing conditions are listed in Table 1. A number of different samples were prepared using the same conditions, to ensure reproducibility. Enriched samples of $^6LiMn_2O_4$, for the variable-temperature NMR experiments, and of $^6Li_2Mn_4O_9$ and $^6Li_4Mn_5O_{12}$ were prepared with ^{6}Li-enriched Li_2CO_3 (Isotec; ^{6}Li > 95%) as one of the starting materials. Otherwise, identical reaction conditions were used. The sample of $Li_2Mn_2O_4$ was prepared by intercalation of $LiMn_2O_4$ (LiMn850) with excess *n*-BuLi in anhydrous hexane at 50 °C for 24 h under an N_2 atmosphere as described in ref 10. A sample with a Li:Mn ratio of 1.1:2 which corresponds to a nominal composition $Li_{1.07}Mn_{1.93}O_4$ was also synthesized at 850 °C, with Li_2CO_3 and Mn_2O_3 as starting materials.

X-ray Powder Diffraction. All of the samples were characterized with a Scintag powder X-ray diffractometer. Diffraction powder patterns were compared with those in JCPDS, confirming the presence of the cubic spinel phase for all of the samples synthesized at high temperatures. No impurity phases were observed except in the case of LiMn550, where a trace of Mn_2O_3 was observed in some but not all of the samples synthesized under these conditions. The presence of a trace amount of Mn_2O_3 in these samples did not produce any discernible differences in the MAS NMR spectra of these samples. Samples of $Li_2Mn_2O_4$ gave powder patterns, which could be indexed to a tetragonal rock-salt diffraction pattern. All of the samples were crystalline, and there did not appear to be any evidence for any amorphous material.

Low-temperature diffraction experiments were performed by using the synchrotron source at the National Synchrotron Light Source at Brookhaven National Laboratory at the X3 (SUNY) beamline (wavelength = 0.500 Å). Experiments were performed on the LiMn550 and LiMn850 samples. The powder X-ray diffraction pattern of LiMn550 did not show any evidence of a cubic-to-tetragonal phase change down to 200 K, the lowest temperature studied. LiMn850 was studied at room temperature and −5 °C. Many of the reflections were observed to split on reducing the temperature to −5 °C, and the new sets of reflections could be indexed to a tetragonal cell. Some cubic phase remained at this temperature, however. Integration of the 400 and 004 reflections showed that ~58% of the sample remained in the cubic phase.

Solid-State NMR Spectroscopy. ^{6}Li and ^{7}Li MAS NMR experiments were performed at 29.47 and 77.83 MHz, respectively, on a CMX-200 spectrometer with double resonance Chemagnetics probes equipped with 5-mm and 3.2-mm rotors for MAS. Spectra were recorded with either single-pulse or echo experiments. Both quadrupolar echoes ($90° - \tau - 90° - \tau -$ acq) and spin-echoes ($90° - \tau - 180° - \tau -$ acq) were used to acquire spectra of some of the materials with broader resonances (e.g., $Li_2Mn_4O_9$ and $Li_4Mn_5O_{12}$); the echo spectra shown were acquired with a quadrupolar echo. Since these echo experiments were performed under MAS conditions, the sequence was rotor synchronized, with values for τ being chosen such that they were multiples of the rotor period (τ = 1/spinning frequency). Note, however, that under rotor-synchronized MAS conditions, the spin-echo experi-

(26) Nayeem, A.; Yesinowski, J. P. *J. Chem. Phys.* **1988**, *89*, 4600.
(27) Cheetham, A. K.; Dobson, C. M.; Grey, C. P.; Jakeman, R. J. B. *Nature* **1987**, *328*, 706. Grey, C. P.; Dobson, C. M.; Cheetham A. K.; Jakeman, R. J. B. *J. Am. Chem. Soc.* **1989**, *111*, 505. Grey, C. D. Phil. Thesis, University of Oxford, 1991.
(28) Liu, K.; Ryan, D.; Nakanishi, K.; McDermott, A. *J. Am. Chem. Soc.* **1995**, *117*, 6897.
(29) Li, J.; Lashier, M. E.; Schrader, G. L.; Gerstein, B. C. *Appl. Catal.* **1991**, *73*, 83.
(30) Carewska, M.; Scaccia, S.; Croce, F.; Arumugam, S.; Wang, Y.; Greenbaum, S. *Solid State Ionics* **1997**, *93*, 227.
(31) Marichal, C.; Hirschinger, J.; Granger, P.; Ménétrier, M.; Rougier, A.; Delmas, C. *Inorg. Chem.* **1995**, *34*, 1773.
(32) Ouyang, B.; Cao, X.; Lin, H. W.; Slane, S.; Kostov, S.; Denboer, M.; Greenbaum, S. G. *Mater. Res. Soc. Symp. Proc.* **1995**, *369*, 59.
(33) Morgan, K. R.; Collier, S.; Burns, G.; Ooi, K. *J. Chem. Soc., Chem. Commun.* **1994**, 1719.
(34) Kumagai, N.; Fujiwara, T.; Tanno, K.; Horiba, T. *J. Electrochem. Soc.* **1996**, *143*, 1007.
(35) Kanzake, Y.; Taniguchi, A.; Abe, M. *J. Electrochem. Soc.* **1991**, *138*, 333.
(36) Mustarelli, P.; Massarotti, V.; Bini, M.; Capsoni, D. *Phys. Rev.* **1997**, *55*, 12018.
(37) Gee, G.; Horne, C. R.; Cairns, E. J.; Reimer, J. Presented at the 40th Rocky Mountain Conference, Denver CO, 1998; *J. Phys. Chem. B*, in press.
(38) Sugiyama, J.; Hioki, T.; Noda, S.; Kontani, M. *J. Phys. Soc. Jpn.* **1997**, *66*, 1187.

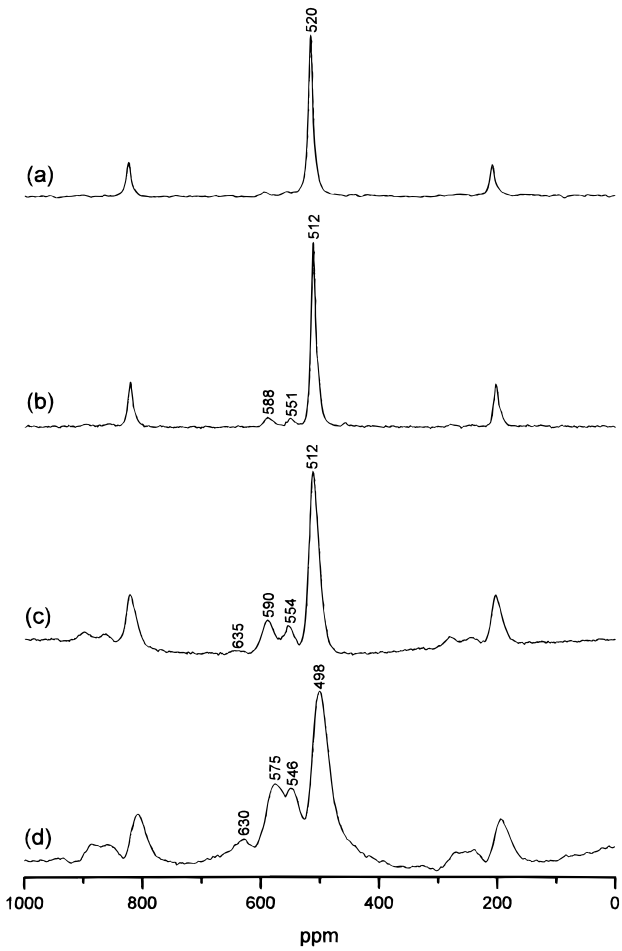

Figure 2. The ^{6}Li MAS NMR spectra of $LiMn_2O_4$ as a function of the firing temperature used to synthesize the sample. (a) LiMn850, (b) LiMn650, (c) LiMn600 and (d) LiMn550. All spectra were acquired with spinning speeds of ~9 kHz.

ment is the more appropriate experiment, due to the refocusing of the first-order quadrupolar interaction under MAS. Thus, the spectra were also subsequently acquired with a spin−echo sequence to ensure that no resonances were missed with the quadrupole-echo sequence. All spectra were referenced to 1 M LiCl solution, at 0 ppm. $\pi/2$ pulses of 2.8 and 2μs were used for ^{6}Li and ^{7}Li, respectively, with delay times of typically 0.2−1 s. ^{6}Li longitudinal relaxation times (T_1s) were measured with an inversion recovery ($180° - \tau - 90° -$ acq) sequence. Variable-temperature spectra were acquired with the Chemagnetics variable temperature stack and with 5-mm rotors. Temperature calibrations performed with $Pb(NO_3)_2$[39] indicated that the real and indicated temperatures differed by no more than 5 °C even at spinning speeds of 9−10 kHz for the temperature range studied. Room-temperature spectra were acquired without the variable temperature stack and without any heater-gas flow over the sample. Under these conditions, the real temperature of the samples is always higher than room temperature and is between 40 and 50 °C.

Results

$LiMn_2O_4$. The ^{6}Li MAS NMR spectra of $LiMn_2O_4$ prepared at different temperatures are shown in Figure 2. All four samples (LiMn850, LiMn650, LiMn600, and LiMn550) show large shifts from the shift position typically obtained for diamagnetic solids at around 0 ppm and large spinning sideband manifolds. X-ray powder diffraction confirmed the presence of the spinel phase and the lack of any impurities. However, the ^{6}Li MAS NMR spectra of the four samples are very different: The ^{6}Li MAS NMR spectrum of LiMn850 (Figure 2 a) is dominated by one major resonance at 520 ppm, which is assigned to lithium in the normal position (8a) of the spinel structure. This is similar to the previously published spectrum by Morgan et al.,[33] where a single isotropic resonance at 520 ppm was also observed, but differs by ~144 ppm from the value of 664 ppm determined by Mustarelli et al.[36] The reason for the difference is unclear, but most likely it results from differences in the spinning speeds used and the difficulty in determining the isotropic resonance of a broad resonance whose isotropic shift is very sensitive to temperature and thus small changes in spinning speed (see below). In contrast, spectra of the samples synthesized at lower temperatures show a number of additional resonances corresponding to several local environments. Three resonances at 512, 551, and 588 ppm are observed for LiMn650 (Figure 2 b), while four resonances are seen for LiMn600 (Figure 2 c) at 512, 554, 590, and 635 ppm, the resonance at 512 ppm being the most intense. The line widths of the resonances increase as the synthesis temperature is lowered, as do the intensities of the higher frequency resonances, four broad resonances being observed for LiMn550 (Figure 2 d) at 498, 546, 575, and 630 ppm. Also noticeable is the small shift of the most intense resonance to lower frequency with decreasing synthesis temperature and the shoulder to low frequency of this resonance that is observed in all of the spectra. T_1 measurements were performed for all of the samples, and values of ~40 ms were determined for the most intense resonance at 512−520 ppm, whereas the smaller resonances at 551−588 ppm had shorter T_1s of, for example, ~30 ms for LiMn650. The ^{6}Li MAS NMR of the sample of $Li_{1.07}Mn_{1.93}O_4$ (not shown) also shows additional smaller resonances at 560, 596, and 648 ppm. The main spinel resonance has shifted slightly from the resonance observed in LiMn850 to 523 ppm.

$Li_4Mn_5O_{12}$, $Li_2Mn_4O_9$, and $Li_2Mn_2O_4$. The ^{6}Li resonances of $Li_4Mn_5O_{12}$ and $Li_2Mn_4O_9$ are observed at higher frequency than those for $LiMn_2O_4$ and are considerably broader (Figure 3 a and b). Only one resonance can be discerned at 687 ppm for $Li_2Mn_4O_9$, however at least two resonances are observed, with isotropic shifts of 847 and 1980 ppm, for $Li_4Mn_5O_{12}$. The shifts of the isotropic resonances are extremely sensitive to temperature, and large shift variations are observed by simply varying the spinning speed. This has been observed before in MAS NMR studies of paramagnetic materials[32,40] and is due to the changes in temperature that arise from frictional heating. Thus the quoted ppm values are accurate to only ~±25 ppm. Both resonances are associated with large spinning sideband manifolds. The sharp resonance at close to 0 ppm results from a very small concentration of a diamagnetic lithium-containing impurity. The spectrum of $Li_2Mn_2O_4$ (Figure 3 c) contains two overlapping resonances at 101 and 118 ppm. The resonance close to 0 ppm results from the unreacted BuLi, which presumably reacts to form Li_2O and Li_2CO_3 on contact with air.

Variable-Temperature ^{6}Li MAS NMR Spectra. The variable-temperature ^{6}Li NMR spectra of LiMn550 − LiMn850 are shown in Figures 4−7. At ambient temperature, all of the spectra show well-resolved peaks. As the temperature increases, all of the resonances shift to lower frequency by ~−120 ppm over 200 °C, and the line widths of the resonances decrease. Considering LiMn550 initially, it is clear that the shift to lower frequencies is accompanied by a collapse of the additional resonances into the larger one assigned to the "normal" spinel lithium environment in $LiMn_2O_4$. By 200 °C, not more than

(39) Ferguson, D.; Haw, J. F. *Anal. Chem.* **1995**, *67*, 3342.

(40) Grey, C. P.; Dobson C. M.; Cheetham, A. K. *J. Magn. Reson.* **1993**, *101*, 299.

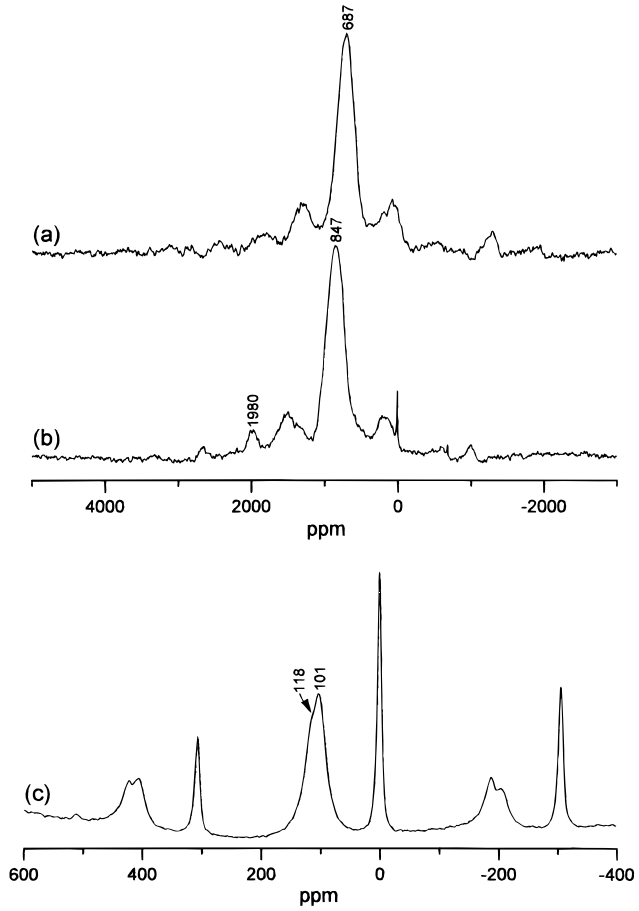

Figure 3. The ^{6}Li MAS NMR spectra of (a) $Li_2Mn_4O_9$, (b) $Li_4Mn_5O_{12}$, and (c) $Li_2Mn_2O_4$ with spinning speeds of ~21 kHz [(a) and (b)] and 9 kHz (c). (a) and (b) were acquired with a rotor-synchronized echo sequence ($\tau = 1$ rotor period). The isotropic resonances of paramagnetic phases are indicated.

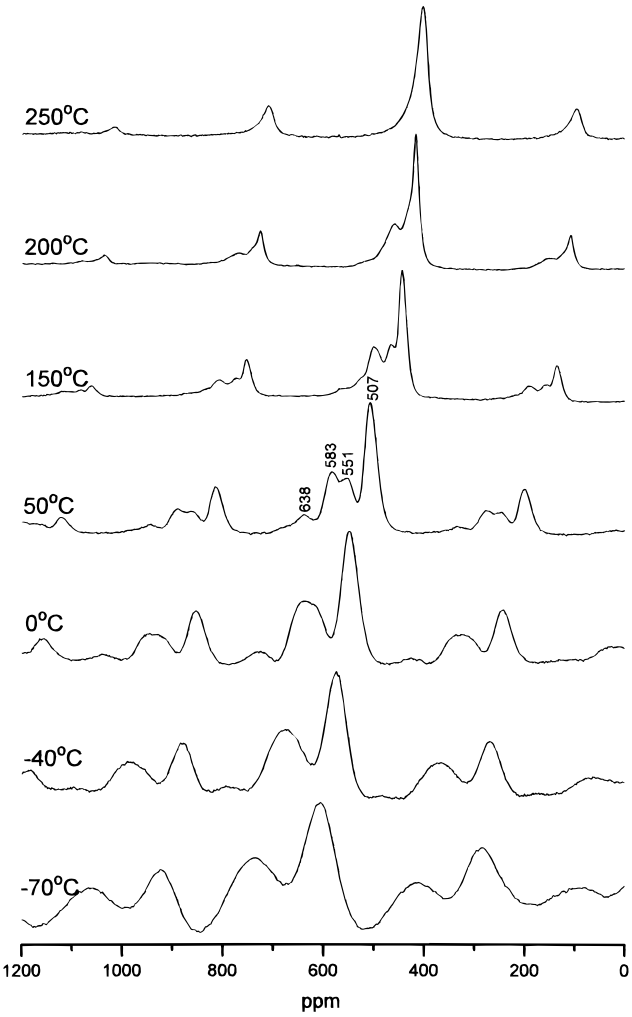

Figure 4. The variable-temperature ^{6}Li MAS NMR spectra of LiMn550 acquired at spinning speeds of ~9 kHz. Isotropic resonances are marked on selected spectra; all other resonances in these spectra are spinning sidebands.

two additional resonances (and a shoulder) are visible, and the relative amount of intensity contained in these smaller resonances has decreased. By 250 °C, only one resonance, with a small shoulder to higher frequency is observed. The behavior of LiMn600 is similar. Small differences are, however, noted. For example, the resonance initially at 586 ppm at 50 °C splits into two resonances by 150 °C. Again, the additional resonances collapse one-by-one into the "normal" spinel resonance. At 250 °C, this resonance and one other smaller broadened resonance remain. Complete coalescence of all of the less intense resonances into the larger resonance is observed for LiMn650 and LiMn850. The shift positions of the "normal" spinel resonance are plotted as a function of inverse temperature in Figure 8, and at temperatures above room temperatures, they show a clear $1/T$ dependence.

The behavior of the samples is very different below room temperature. The resonances from the LiMn550 and LiMn600 broaden at lower temperature and shift to higher frequencies, as expected. No sharp discontinuities in the shift position with temperature are observed. However, abrupt changes in the spectrum of LiMn650, are observed below −10 °C. Three intense resonances are observed at 488, 647, and 709 ppm (at −40 °C), which account for considerably more intensity than the smaller additional resonances that were seen at higher temperatures. Similar behavior is observed for LiMn850, where again three additional resonances (and a shoulder) are observed. Since the concentration of the smaller resonances was close to negligible in this sample at higher temperatures, the additional resonances seen at low temperatures must arise from a different mechanism. These resonances start to appear at 5 °C, and have increased in intensity, relative to the resonance from the "normal" spinel environment, in the spectrum acquired at 0 °C. Very little difference in intensity of these resonances is observed on lowering the temperature further to −70 °C. The LiMn850 sample showed a cubic-to-tetragonal phase transition, in the X-ray diffraction studies, due to the Jahn−Teller distortion; this phase transition appears to be associated with the formation of these new resonances. The presence of the "normal" spinel resonance, even at the lowest temperatures studied, is consistent with our and previous[41] diffraction results where the cubic phase is still detected below the phase transition. Also noteworthy is the deviation of the shift from the "normal" spinel from a $1/T$ dependence (see Figure 8), even for the compounds where no evidence for a static JT distortion is observed.

^{7}Li MAS NMR spectra of LiMn550 and LiMn600 were acquired at room and higher temperatures, to investigate the effect of the difference in the gyromagnetic ratio of ^{6}Li and ^{7}Li on their variable-temperature MAS NMR spectra. The ^{7}Li MAS NMR spectra of LiMn550 are shown in Figure 9. At the spinning speeds used, only three resonances can be discerned at 50 °C, at 511, 553, and 586 ppm. Since this sample differs from the LiMn550 sample (which was enriched in ^{6}Li) used

(41) Yamada, A.; Tanaka, M. *Mater. Res. Bull.* **1995**, *30*, 715.

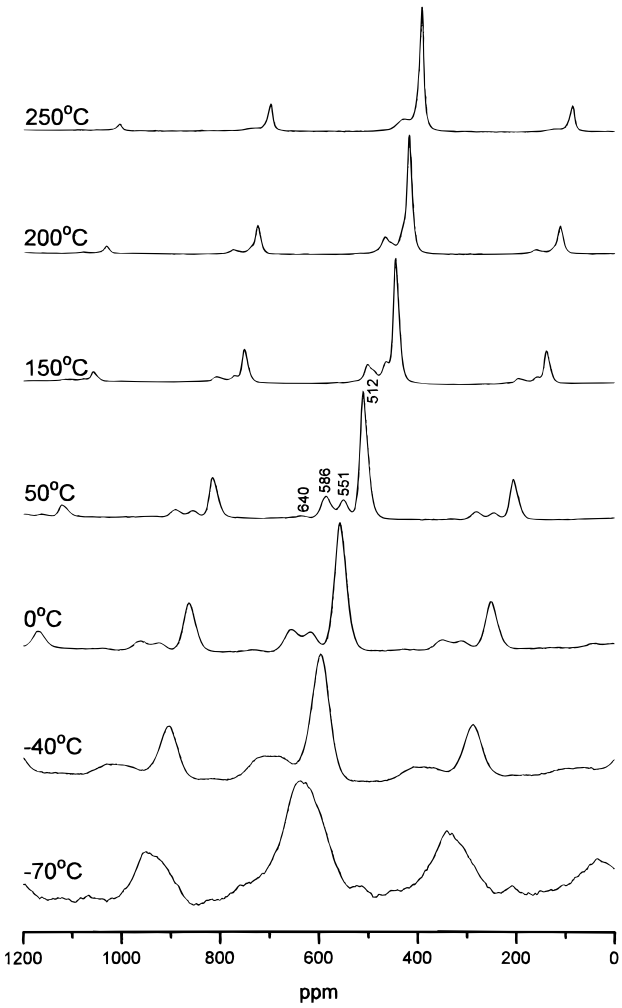

Figure 5. The variable-temperature ^{6}Li MAS NMR spectra of LiMn600 acquired at spinning speeds of ∼9 kHz.

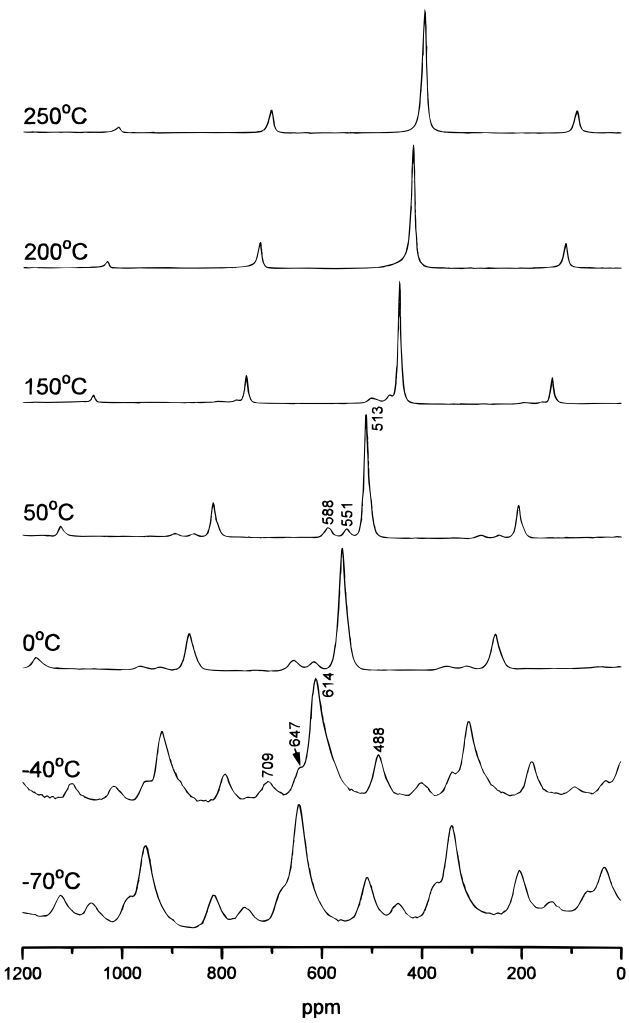

Figure 6. The variable-temperature ^{6}Li MAS NMR spectra of LiMn650 acquired at spinning speeds of ∼9 kHz.

for the ^{6}Li studies, ^{6}Li MAS NMR spectra were also acquired for this sample. No discernible differences were observed between the ^{6}Li NMR spectra of this sample and those reported in Figures 2 and 4. The smaller, less intense, resonances (at ∼638 ppm at 50 °C) are not observed in the ^{7}Li spectrum of LiMn550; these resonances are presumably located under the spinning sidebands of the more intense resonances, but were observed at fast spinning speeds (∼24 kHz) in other samples. The slower spinning speed, the broader resonances, and the overlap of the isotropic resonances and sidebands, account for the differences in apparent intensity of the three observed resonances, in comparison to the relative intensities of these resonances in the ^{6}Li MAS NMR. Under these conditions, it is difficult to determine the position of the baseline of the resonances. Spectra with relative intensities for the resonances close to those seen in the ^{6}Li MAS NMR spectra were obtained with a different MAS probe, at fast spinning speeds (>20 kHz). The small differences in chemical shift between the ^{7}Li and ^{6}Li spectra of LiMn550 are most likely due to small differences in the real temperature of the sample, which are estimated to be no more than ±5 °C, on the basis of calibration studies. As in the ^{6}Li MAS NMR of LiMn550, the resonance originally at 553 ppm at 50 °C shifts close to the main resonance (originally at 511 ppm), as the temperature increases, and by 200 °C is only visible as a shoulder of the main resonance. By 250 °C, only the main resonance with a shoulder to higher frequency is observed. The collapse of the two smaller resonances into the main resonance occurs at the same temperature, within experimental error, in the ^{6}Li and ^{7}Li NMR spectra. ^{7}Li MAS NMR spectra were also acquired for LiMn600. Again, the shifts of the ^{7}Li resonances were essentially identical to those observed in the ^{6}Li MAS NMR spectra. As in the ^{6}Li MAS NMR spectra, the resonance at ∼550 ppm at 50 °C is only observable as a shoulder of the main resonance at ∼200 °C, and by 250 °C is no longer visible. The resonance originally at ∼585 ppm shifts toward the main spinel resonance, splits, and then broadens but is still visible at 250 °C.

Discussion

The ^{6}Li MAS NMR spectra of $LiMn_2O_4$ are extremely sensitive to the different synthesis conditions. Several resonances are observed in the ^{6}Li MAS NMR spectra for the low-temperature preparations, indicating that there are several different lithium local environments. Both the formation of the defect spinel (with vacancies on both the lithium and manganese sites) and the oxidation state of the manganese have been shown to be highly dependent on temperature, spinels with higher manganese oxidation states and more defects being preferentially formed at lower temperatures.[13] The ^{6}Li MAS NMR spectra are consistent with this, the intensity of the resonances other than that assigned to Li^+ in the normal spinel environment (at 512−520 ppm) increasing as the synthesis temperature is decreased.

The stoichiometric $LiMn_2O_4$ spinel contains both Mn^{4+} (d^3) and Mn^{3+} (high spin d^4) ions in a 1:1 ratio, and is a hopping

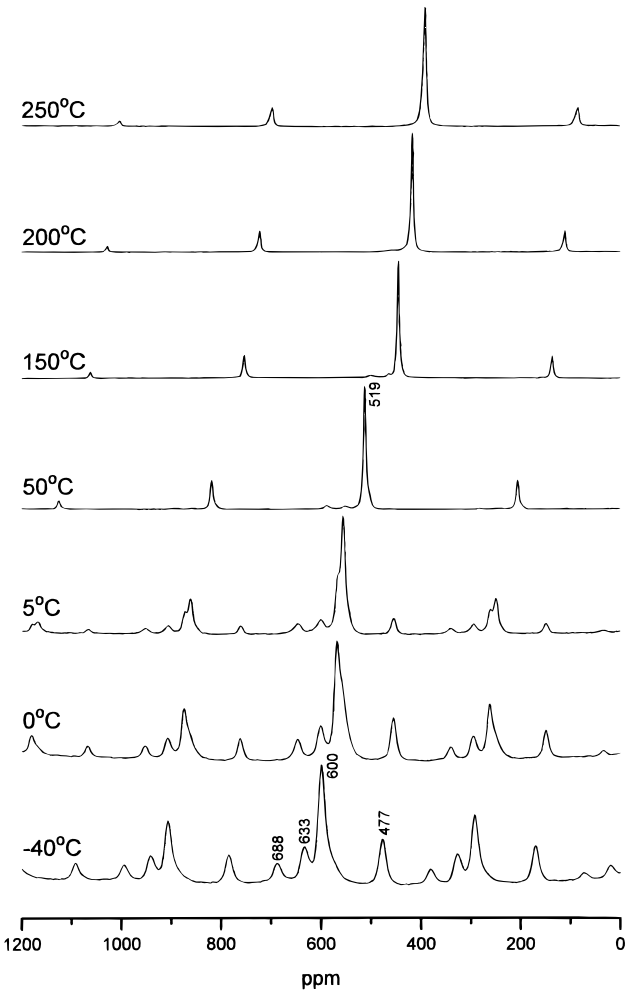

Figure 7. The variable-temperature [6]Li MAS NMR spectra of LiMn850 acquired at spinning speeds of ~9 kHz.

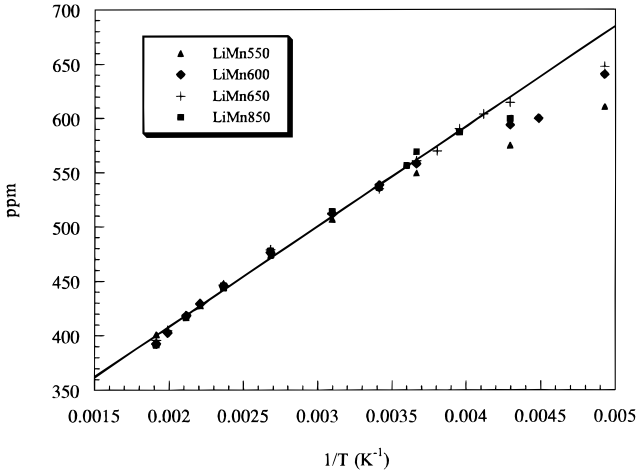

Figure 8. A plot of the [6]Li NMR shift of the resonance assigned to the normal spinel environment, as a function of $1/T$ for LiMn550, LiMn600, LiMn650, and LiMn850. The linear curve fit to the experimental data is shown (solid line).

semiconductor in which (unpaired) electrons in the e_g orbitals in Mn^{3+} hop to neighboring Mn^{4+} ions.[7,8,15] Hopping is limited to orbitals of the same energy (e.g., the e_g orbitals of metals on the same site). This hopping is fast in the time scale of the NMR experiment, and thus, the lithium NMR shifts are sensitive only to the average charge of the manganese (i.e., 3.5 for the stoichiometric material). Thus, only one resonance is predicted

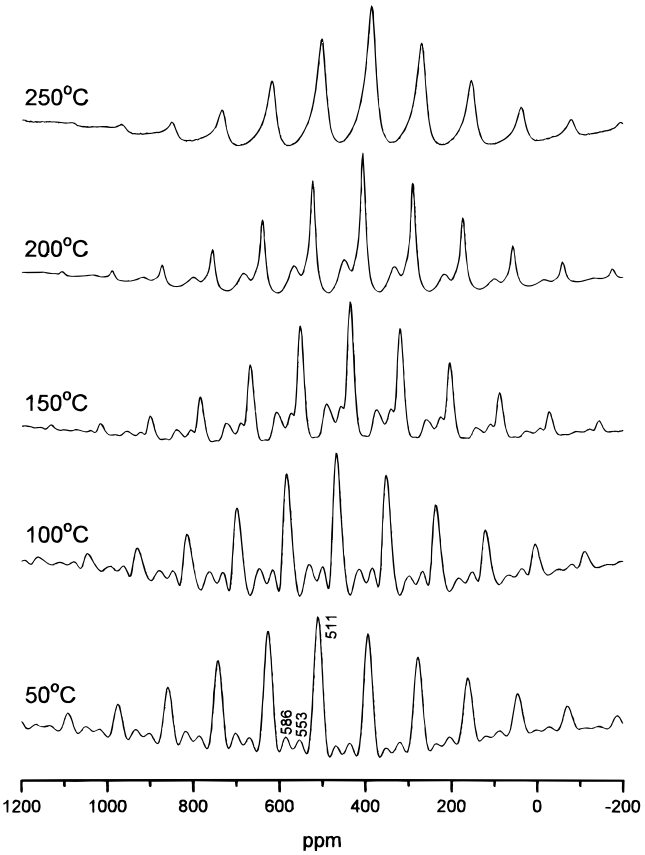

Figure 9. The variable-temperature [7]Li MAS NMR spectra of LiMn550 acquired at spinning speeds of ~9 kHz. Isotropic resonances are marked on the spectrum acquired at 50 °C. All other resonances in this spectrum are spinning sidebands.

for the stoichiometric material, consistent with the spectrum of LiMn850, which essentially contains only one resonance. Furthermore, a change in the stoichiometry of the spinel, and thus a change in the average oxidation state of manganese, is expected to result in a shift of the resonance.

The [6]Li NMR spectra show a large shift to high frequency with increasing Mn oxidation state, and shifts of 847 and 1980 ppm are observed for the two resonances of $Li_4Mn_5O_{12}$ (Mn^{4+}) and ~687 ppm for $Li_2Mn_4O_9$ (Mn^{4+}), in comparison to a shift of 520 ppm for $LiMn_2O_4$ (oxidation state ≈ 3.5). A shift to lower frequencies is observed on decreasing the oxidation state to 3.0, and resonances are observed at 101 and 118 ppm for $Li_2Mn_2O_4$. This initially appears counterintuitive since the Mn(IV) materials have a lower effective magnetic moment[13] and do not contain any electrons in the e_g orbitals. However, we can conclude that an increase in manganese oxidation state from (III) to (IV) results in a shift to higher frequency for the samples and lithium and manganese local environments studied. Furthermore, the center of gravity of the resonances shifts to higher frequencies, with decreased synthesis temperature, for the samples LiMn850 through LiMn550. This is consistent with the increase in the manganese oxidation state, which occurs in these 1:2 Li:Mn spinels on lowering the synthesis temperature.[13] To understand the cause of the shifts and the large variations in more detail we need to consider the local environment for lithium in these and related materials and the possible shift mechanisms.

Shift Mechanisms. There are two important interactions that govern the NMR spectra of paramagnetic materials, one involving a through-space, dipolar interaction between the nuclear and electronic moments and the other involving a

through-bond (Fermi-contact) interaction. The Fermi-contact shift is a measure of the unpaired electron spin density from the paramagnet that is transferred to the nucleus of the NMR active spin (via the occupation of the s orbital). The isotropic part of the interaction can be written as[42]

$$H_c = I_z A_s \langle S_z \rangle \quad (1)$$

where A_s is the electron−nuclear hyperfine coupling constant and $\langle S_z \rangle$ the thermally averaged value of the paramagnetic spin. The sign of A_s determines the sign of the spin density transferred to the s orbitals of the resonant atom, and thus the direction of the shift, and will depend on the nature of the overlap between the orbitals containing the unpaired electrons and the s orbitals. The magnitude of A_s controls the size of the shift. Since $<S_z>$ is proportional to χB_o, where χ is the susceptibility and B_0 the field, the Fermi-contact shift shows the same temperature dependence as the magnetic susceptibility and will scale with the field (in absolute frequency units). The magnetic susceptibility of these systems shows a Curie-like behavior above 83 K in one report[13] and 40 K in a second[38] consistent with the $1/T$ temperature behavior of the shifts observed for all of the resonances of LiMn550, LiMn600, LiMn650, and LiMn850 (Figure 8).

The second important mechanism, the through-space dipolar interaction, H_{en}, between the nuclear (μ_N) and electronic magnetic moments is similar to the dipolar interaction between nuclear spins[26,43]

$$H_{en} = \mu_e \mathbf{D}_{en} \mu_N \mu_0 / 4\pi \quad (2)$$

where $\mathbf{D}_{en}$ is the dipolar coupling tensor. μ_e, the time-averaged electronic moment, can be rewritten in terms of the atomic susceptibility χ_A (the susceptibility of a paramagnet)

$$\mu_e = \chi_A B_0 / \mu_0 \quad (3)$$

The anisotropic part of the interaction is the primary cause of the large spinning sideband manifolds observed for paramagnetic solids.[26] Furthermore, the larger value of μ_N for ^{7}Li, in comparison to ^{6}Li, results in the much larger spinning sideband manifolds in the ^{7}Li MAS NMR spectra. When the susceptibility is isotropic, this mechanism does not cause a shift. However, if the susceptibility is anisotropic, a small shift will be observed, which is often referred to as the pseudocontact shift. Note that although the bulk susceptibility of a cubic material cannot be anisotropic, the atomic susceptibility may be anisotropic if the local symmetry at the site of the paramagnet deviates from cubic symmetry. This is the case for the manganese site in the spinel structure, which has trigonal site symmetry. Since the isotropic part of the susceptibility is typically much larger than the anisotropic part, the pseudocontact shift is generally small in comparison to the size of the sideband manifolds. Note, however, that this statement will not always hold for coupling to more than one paramagnetic spin, since the dipolar field will then be the sum of all the individual coupling matrixes defined in eq 2 and some cancellation may occur, depending on the arrangement of the paramagnets around the nucleus. Pseudocontact shifts are also typically an order of magnitude smaller than the shifts observed here and do not necessarily show an inverse temperature relationship.[43,44] Furthermore, the spin−orbit coupling constants are small for Mn^{3+} and Mn^{4+},[45] and only small pseudocontact shifts are predicted.

A shift mechanism that is important in metals is the Knight shift. This results from the coupling of the magnetic moments of the (unpaired) conduction electrons at the Fermi level to the nuclear moment and depends on the density of states at the Fermi level.[46] It is more appropriate, however, to view the electrons in the e_g orbitals that are responsible for conduction as being localized. Under these conditions, the electronic conductivity is no longer temperature independent, and there is an activation barrier to conduction associated with the movement of the electron from the low- to the high-valence cation. This behavior has been observed experimentally.[46,47] The susceptibilities of these materials are consistent with localized electrons, in agreement with this. The Knight shift will be small or negligible for these hopping semiconductors. Thus, to a first approximation, the Knight-shift and dipolar-shift mechanisms can be excluded, and shifts are expected to be dominated by a Fermi-contact mechanism: This is consistent with the observed temperature behavior in these systems and is in agreement with the conclusions of the earlier ^{7}Li MAS NMR study.[36] There is clearly a temperature-independent component to the shift since the plots of shift versus $1/T$ do not pass through the origin. This additional contribution to the hyperfine shift may result from the mixing in of excited (electronic) states.[45]

The size of the hyperfine-coupling constant, A_s, depends on the overlap integral, which is itself a function of the overlap between the s orbital at the lithium atom, and the t_{2g} and e_g orbitals of the manganese atom. This overlap can either occur directly or via the intervening coordinated oxygen atoms. It is this hyperfine interaction that determines the size and type of coupling (ferromagnetic versus antiferromagnetic) in magnetic systems, except that in NMR the coupling must involve the s-orbital at the site of the nucleus, which is not a requirement for coupling between two electronic spins. The magnetic coupling in spinels has been widely studied, and a variety of overlap mechanisms have been determined,[48−50] which depend on whether the t_{2g} or e_g orbitals are involved. It is useful to briefly review a number of these mechanisms since they provide insight into the possible sources of the NMR shifts. For Mn−Mn coupling involving Mn^{3+} and Mn^{4+} ions on the B (16d) site of the spinel structure, two types of coupling mechanisms are important: (i) an antiferromagnetic Mn−Mn interaction, which occurs via the direct overlap of t_{2g} orbitals across a common octahedral edge and (ii) Mn−O−Mn superexchange interactions mediated by the intervening oxide 2p orbitals. Figure 10 shows the local environment for manganese in the 16d site of the spinel structure. The manganese (16d)−oxygen octahedra share common edges, and thus the manganese ions are connected via Mn−O−Mn bridges with ∼96° bond angles. Mechanisms resulting in the largest exchange coupling involve coupling between electrons in a filled oxygen 2p orbital and the adjacent manganese t_{2g} orbital (Mn^{3+} or Mn^{4+}) to form a π bond. Overlap between the 2p oxygen and an e_g orbital of the second manganese orbital can then occur via a σ bonding arrangement. If the σ interaction involves Mn^{3+} ions with partially filled e_g orbitals, this results (by either a delocalization or correlation

(42) McConnell, H. M.; Robertson, R. E. *J. Chem. Phys.* **1958**, *29*, 1361.
(43) Kurland, R. J.; McGarvey, B. R. *J. Magn. Reson.* **1970**, *2*, 286.
(44) Bleaney, B. *J. Magn. Reson.* **1972**, *8*, 91.
(45) Figgis, B. N. *Introduction to Ligand Fields*; John Wiley & Sons: New York, 1966.
(46) Slichter, C. P. *Principles of Magnetic Resonance*; Springer-Verlag: New York, 1989; Chapter 4.
(47) Bloembergen, N. *Physica* **1954**, *20*, 1130.
(48) Goodenough, J. B. *Magnetism and the Chemical bond*; John Wiley & Sons: New York, 1963; Chapter III.
(49) Goodenough, J. B.; Loeb, A. L. *Phys. Rev.* **1955**, *98*, 391.
(50) Anderson, P. W. *Phys. Rev.* **1959**, *115*, 2.

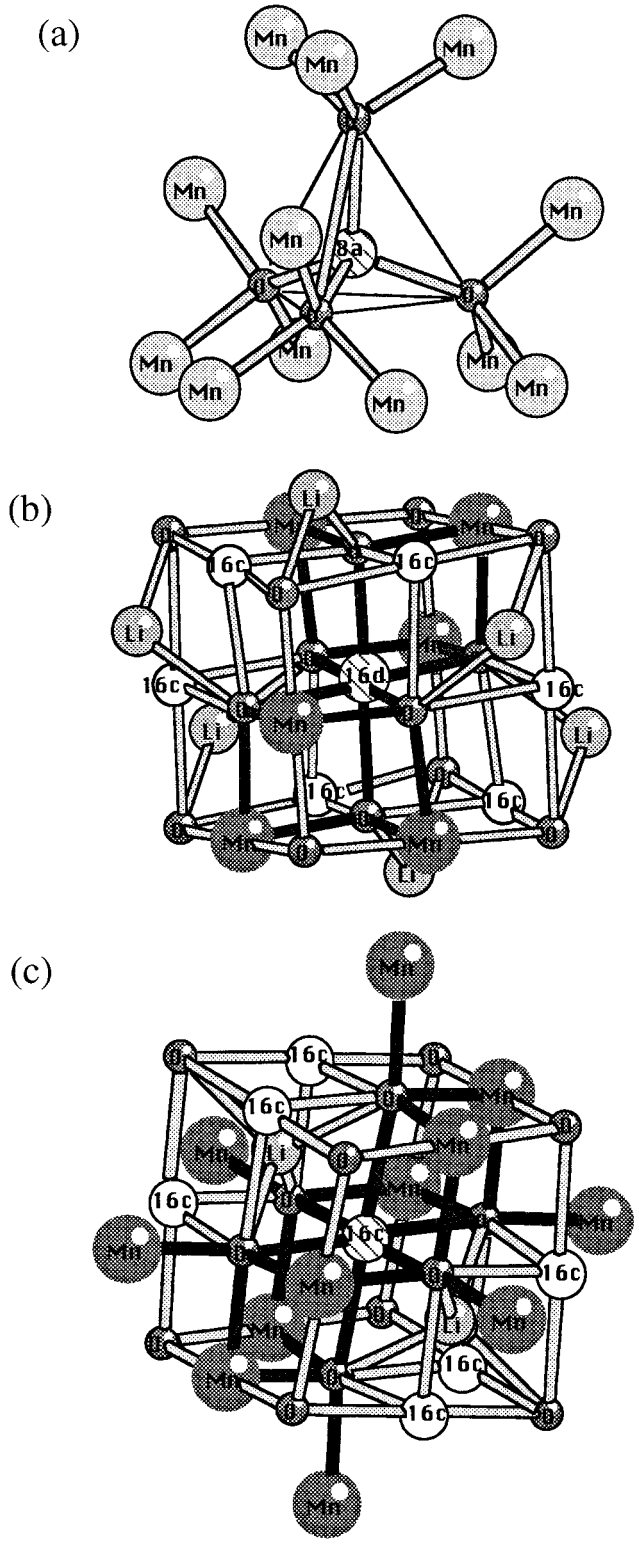

Figure 10. The local coordination environment of the lithium and manganese ions (or vacancies) in the spinel structure. (a) The lithium ion in the 8a site. (b) The 16d site typically occupied by manganese. (c) A 16c octahedral vacancy. The M−O−Mn bonds from the central atom or vacancy (M = 8a (Li), 16d, or 16c cations) are shaded.

superexchange mechanism[48]) in spin magnetization in the e_g orbitals with the sign opposite to that in the t_{2g} orbitals of the first manganese ion. Thus, an antiferromagnetic interaction between the two manganese spins results. In contrast, if the e_g orbital is empty (e.g., for Mn^{4+}−O−Mn^{4+} superexchange), magnetization of the same sign is induced in this orbital. Alignment of the spins in the half-filled t_{2g} and the e_g orbitals of the second manganese atom, in the same direction, results in an overall ferromagnetic coupling between the two manganese electronic spins. Antiferromagnetic coupling is predicted for $LiMn_2O_4$ by both direct overlap of the manganese orbitals and antiferromagnetic Mn^{3+}−O−Mn^{4+} superexchange; this has been observed experimentally.[13,38] Ferromagnetic ordering is, however, observed in $Li_4Mn_5O_{12}$, due to Mn^{4+}−O−Mn^{4+} 90° ferromagnetic interactions. Magnetic coupling between the A and B sites in spinels has also been extensively studied. Coupling mechanisms involving angles other than 90 or 180° are now involved (approximately 125°), and the overlap between larger numbers of orbitals (metal and oxygen) needs to be considered.

Table 2. Local Environment for Lithium, and Nominal Oxidation State, in a Variety of Lithium Manganates[a]

compd	site	no. of Li−O−M bonds	bond angle (deg)	Mn oxidn state	NMR shift (ppm)
$Li_4Mn_5O_{12}$	8a	12	121.0	4	847
	16d	12	96.2 ± 0.3		1980
	(16c)	(6)	(171.9)		
		(12)	(89.6)		
$Li_2Mn_4O_9$	8a	12	120.7	4	687
Li_2MnO_3	4h	4	180	4	905/850[b]
		8	90		
	2b	12	90		1817/1770[c]
	2c	4	180		922/875[c]
		8	90		
$Li_2Mn_2O_4$	8a	12	122.3	3	
	16c	6	176.7 ± 0.2		118, 101
		12	89.9		

[a] M denotes a cation in the 16d site of the spinel structure. M may also be a cation vacancy in the case of $Li_2Mn_4O_9$. the NMR assignments are discussed in the text. Two values for the shifts are given for Li_2MnO_3, the first coming from ref 33 and the second from ref 36. [b] Assignment from ref 33, based on the intensity of the resonance. [c] Assignments consistent with refs 33 and 36.

Similar mechanisms for the transfer of spin polarization from the induced magnetic moment at the manganese ion, in a magnetic field, to the lithium s-orbitals can be envisaged by considering the local environment surrounding the lithium ions (e.g., Figure 10) in the different structures. The compounds containing Mn^{4+} only (i.e., empty e_g orbitals) will be considered initially, before the effect of the partially filled e_g orbitals is discussed.

Mn(IV) Compounds. Earlier ^{6}Li and ^{7}Li MAS NMR of the rock-salt type phase Li_2MnO_3 showed three resonances at 905, 922, and 1817 ppm, in one study,[33] and 850, 875, and 1770 ppm in the second.[36] This material contains Mn^{4+} and a combination of close-to-linear and bent (90°) Li−O−Mn bonds (see Table 2). The resonance at 905 ppm has been assigned to the 4h site, on the basis of intensity. The resonance 922/875 ppm can then be assigned to the 2c site, since it has a similar lithium local environment. Thus, the resonance at 1817/1770 is assigned to the 2b site. Analogous arguments were made in ref 32 to make the same assignments. The lithium site containing 12 Li−O−Mn 90° (2b) bonds results in the largest shift (∼1800 ppm from the typical chemical shift position of a diamagnetic compound at ∼0 ppm). Assuming that we can break the shifts down into individual contributions from different Li−O−Mn bonds and that the shifts are primarily caused by paramagnets in the first cation coordination sphere of Li^+, each Li−O−Mn bond results in a shift of ∼150 ppm. The assumption of a shift of 0 ppm for the diamagnetic compound is justified, given the small chemical shift range for diamagnetic compounds and the very large shifts due to the paramagnets. Evidence for the assumption that shifts are additive, depending on the total

numbers of manganese in the local coordination sphere, comes from the very similar shifts observed for two of the resonances (assigned to the 4h and 2c sites). For a lithium ion in the 4h and 2c sites, with eight 90° Li−O−Mn bonds, the total contribution to the shift from the Li−O−Mn 90° bonds is ∼1200 ppm. Thus, the shift resulting from the linear Li−O−Mn bonds, of which there are four, is opposite in sign and is ∼−75 ppm per 180° Li−O−Mn bond.

Each lithium ion in the 8a site of the spinel structure is coordinated to four oxygen atoms, which are in turn coordinated to three manganese ions (Figure 10 a). Thus, there are 12 Li−O−Mn bent bonds. Refinement of the structure of $Li_4Mn_5O_{12}$ showed that the additional lithium ions substitute for manganese in the 16d site.[4,19,21] Each 16d lithium ion is coordinated to six other 16d sites via 12 Li−O−(16d Mn/Li) bonds with a bond angle of close to 90°(Figure 10 b). Note that for materials with such high lithium content, a lithium ion in a 16d site may be surrounded by other lithium ions in adjacent 16d sites, and thus there may be fewer than six manganese ions in the local coordination sphere. The resonances at 847 and 687 ppm of $Li_4Mn_5O_{12}$ and $Li_2Mn_4O_9$, respectively, are both assigned to lithium in the 8a site. On that basis, the resonance at 1980 ppm in $Li_4Mn_5O_{12}$ is assigned to lithium in the 16d site. Differences in the shifts for the two 8a sites will arise from the different numbers of manganese ions in the Li^+ local coordination sphere. The ideal $Li_2Mn_4O_9$ structure can be written as $(Li_{0.89}\square_{0.11})$-$[Mn_{1.78}\square_{0.22}]O_4$, where □ denotes a vacancy. Thus, there will be, on average, fewer than 12 manganese ions in the local coordination sphere. Assuming a random distribution of vacancies, the probabilities of 0, 1, and 2 vacancies in the lithium coordination sphere are 24.7, 36.6, and 24.9% respectively. Assuming that each Li−O−Mn bond gives rise to a discrete shift in the lithium NMR resonance, a broad resonance is predicted, as observed. The maximum of the resonance should correspond to the shift for lithium surrounded by around 11 manganese ions. Thus, each Li−O−Mn (bent) bond contributes a shift of ∼+62 ppm. The ideal $Li_4Mn_5O_{12}$ material can be written as $Li[Li_{0.33}Mn_{1.67}]O_4$, and again, there are fewer manganese ions in the local coordination sphere of the 8a lithium cations. Again, the shift should be expected to be sensitive to lithium substitution in the 16d site, and the shift is expected to shift to lower frequency as the amount of lithium substitution increases. It is not clear, therefore, why a larger shift is observed for the 8a cations in this material, in comparison to the shift for $Li_2Mn_4O_9$. Although it is difficult to estimate this accurately, given the signal-to-noise ratio and large numbers of sidebands, the ratio of the intensity of the resonances at 847 ppm to the resonance at 1980 ppm appears to be considerably more than 3:1, and our material does not appear to contain as much doping in the 16d site as predicted for the ideal material. In addition, a small amount of residual Mn^{3+} may be present in $Li_2Mn_4O_9$, which could affect the position of the NMR resonance. Another possibility is that there are changes in Li−O−Mn bond lengths and angles between these two compounds. However, the unit cell parameter of $Li_4Mn_5O_{12}$ (8.14 Å)[4,21] is only slightly smaller than that for $Li_2Mn_4O_9$ (8.17 Å).[4,20]

Lithium in the 16d site, which resonates at 1980 ppm, contains six 16d ions in its local coordination sphere (Table 2, Figure 10). This local environment is almost identical to the 2b site in Li_2MnO_3, and similar shifts are observed, consistent with the assignment. Again, assuming that lithium substitution in the 16d site of the spinel structure is less than the theoretical 33%, each Mn^{4+} ion (i.e., 2 Li−O−Mn 90° bonds) contributes a shift of ∼330 ppm. The smaller shift observed for Li_2MnO_3 (300 ppm) may be a consequence of slightly different bond angles and lengths: e.g., Li−O bond lengths of 2.06[51] and 1.94 Å[21] are reported for Li_2MnO_3 and $Li_4Mn_5O_{12}$, respectively.

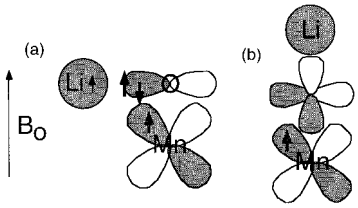

Figure 11. (a) A schematic diagram showing how spin polarization of the same sign in transferred from a t_{2g} orbital on the manganese atom via a filled 2p orbital on an adjacent oxygen atom, in the presence of an external magnetic field, represented by B_o, via a Li−O−Mn 90° interaction. If the Li−O−Mn bond is linear, as shown in (b), there is no direct mechanism for overlap involving the t_{2g} orbitals, the oxygen 2p (and s) orbitals and the unoccupied Li^+ 2s orbital.

The similar shifts for different local environments provide additional evidence that the shifts are not dominated by pseudocontact shifts. The sign of the pseudocontact shift depends on θ, the angle the Mn−Li interatomic vector makes with the principal axis of the atomic susceptibility tensor (i.e., $\chi_{||}$) (defined by the site symmetry at the manganese site) through the angular relationship $(3\cos^2\theta - 1)$.[43] For the spinel, $\chi_{||}$ is oriented along the ⟨111⟩ direction. This is unlikely to be the case for Li_2MnO_3 which crystallizes in a monoclinic space group (C_2/m).[51] Thus, similar pseudocontact shifts for the 16d site in $Li_4Mn_5O_{12}$ (where $3\cos^2\theta - 1 \approx -1$) and the 2b site in Li_2MnO_3 are extremely unlikely.

Returning to the mechanisms of superexchange in magnetic systems, the largest coupling for transition-metal cations connected by M−O−M bonds with a 90° bond angle occurred via the direct overlap of the t_{2g} orbitals. By analogy, one possible shift mechanism here involves direct overlap of the half-filled t_{2g} orbitals and the empty lithium 2s orbitals. Direct transfer of spin polarization to the lithium, with the same sign as at the Mn^{4+}, is predicted. This should result in a positive shift. Overlap involving a π interaction between the t_{2g} orbital and a 2p orbital at the intervening oxygen will also result in a positive shift: Polarization of opposite sign is transferred from the filled 2p oxygen orbital to the t_{2g} orbital, and thus net magnetization of the same sign as that at the Mn^{4+} ion is transferred from the 2p oxygen orbital to the lithium ion. This is shown schematically in Figure 11 a.

The e_g metal orbitals, which point directly toward the oxygen atom, are unoccupied, and there is no direct overlap mechanism involving the half-filled t_{2g} orbitals, for a linear Li−O−Mn^{4+} bond (Figure 11 b). A smaller shift is observed in the ^{6}Li NMR, consistent with this. Two possible mechanisms resulting in unpaired spin density at the lithium nucleus can be envisaged: Transfer of spin polarization can occur indirectly either via a π interaction between the t_{2g} orbital, the intervening oxygen 2p orbital, and a Li^+ 2p orbital or via a σ interaction involving the empty e_g orbitals (and 2s (Li^+) and 2p (O) orbitals). A mechanism similar to the latter interaction has been shown to be important in controlling the Fermi-contact shifts due to lanthanide ions in the early part of the 4f series, where spin density is transferred into the empty 6s and 6p orbitals of lanthanide ions and the 4f orbitals are not directly involved.[52] For e_g orbitals that are less than half-filled, this latter mechanism, by analogy with similar superexchange mechanisms, should

(51) Strobel, P.; Lambert-Andron, B. *J. Solid State Chem.* **1988**, *75*, 90.
(52) Watson, R. E.; Freeman, A. J. *Phys. Rev.* **1967**, *156*, 251.

result in the transfer of negative spin density into the Li^+ 2s orbital,[48] consistent with the sign of the observed hyperfine shift.

Compounds Containing Both Mn^{3+} and Mn^{4+}. Considering only LiMn850 initially, it is clear that addition of electrons into the e_g orbitals causes a shift to negative frequencies (from ~847 to 520 ppm), and a smaller overall shift in comparison to the other Mn^{4+} spinels. This is initially counterintuitive since the number of unpaired electrons is greater for LiMn850. This confirms, however, that different shift mechanisms must operate for interactions involving the e_g and t_{2g} orbitals. As before, the t_{2g} orbitals should interact with the adjacent 2p oxygen orbitals producing a positive shift. The e_g (d_{z^2} or $d_{x^2-y^2}$) orbitals can interact with a perpendicular 2p oxygen orbital in a σ-bonding arrangement. This must result in a negative shift, possibly via the transfer of electron density from the 2p oxygen orbitals to the partially filled e_g orbitals (as was proposed for Mn(IV) compounds). The decrease in covalency of the Mn−O bond, on adding electrons to the (antibonding) e_g orbitals, will also reduce the size of the hyperfine interactions, as has recently been suggested by Gee et al.[39] The shift from the shift position for the 8a sites in $Li_4Mn_5O_{12}$ should depend on the number of electrons in the e_g orbitals. Thus, assuming an oxidation state of 3.5 for manganese in LiMn850, a shift of ~−327 ppm occurs on adding 0.25 electrons per e_g orbital to the manganese ions.

Mn^{3+} Materials. Much smaller shifts are observed for materials containing Mn^{3+} ions, resonances being observed at 100−160 ppm for $Li_2Mn_2O_4$ and $LiMnO_2$. The shift to lower frequencies is consistent with the shift difference between the Mn^{4+} and the mixed Mn^{3+}/Mn^{4+} compounds. Two poorly resolved resonances were observed for $Li_2Mn_2O_4$ at 101 and 118 ppm. The neutron diffraction study of this material has shown that the Li^+ cations reside on both the 8a and 16c sites of the spinel structure in this material, despite the very close proximity of the 8a and 16c sites.[9] The differences in the shifts observed for lithium in the 8a sites of LiMn850 and $Li_4Mn_5O_{12}$ of −327 ppm suggest that lithium in the 8a site of a Mn^{3+}-containing material should resonate close to 193 ppm, close to the experimentally observed shifts. Thus, the less intense resonance at 118 ppm is tentatively assigned to this site, while the more intense resonance is assigned to the 16c site. The occupancy of the 16c site was only ~79%, while the 8a occupancy was only 43%, in the neutron diffraction study.[9] We are currently exploring the effect of electrochemical insertion and deintercalation in this system to examine the effect of percentage substitution on the chemical shift positions and intensities of these two resonances.

The Disordered Spinels LiMn550, 600, 650, and $Li_{1.07}Mn_{1.93}O_4$. At least four additional resonances are observed in these phases that cannot be assigned to the normal lithium environment in the spinel. There are a number of possible sites in the spinel structure, which could accommodate lithium ions and give rise to different ^{6}Li and ^{7}Li resonances, i.e., the 16c (octahedral), 48f, and 8b (tetrahedral) vacancies, or the 16d manganese site. Ammundsen et al. have calculated the energies for lithium substitution in the unoccupied tetrahedral and octahedral sites of λ-MnO_2 with atomistic simulation methods[53] and have obtained energies of −7.86, −6.76, −3.12, and +10.49 eV for substitution into the 8a, 16c, 48f, and 8b sites, respectively. Thus the 8a tetrahedral site is predicted to be the most favorable for Li^+ occupation, consistent with the structure of the normal spinel $LiMn_2O_4$ structure. However, the 16c octahedral and 48f tetrahedral sites are also energetically favorable. They also calculated the energetics for excess lithium substitution in the presence of a manganese 16d vacancy and obtained the following values: 8a + 16d (−9.77 eV), 8a + 16c (−7.44 eV), 16c + 16d (−2.90 eV).[53] Thus, the most stable configuration is found when the excess lithium ions substitute into the 16d manganese vacancies and the other lithium ions remain in their normal 8a sites. This is consistent with the structure obtained for $Li_4Mn_5O_{12}$. (Note the negative enthalpy calculated for 8a + 16c, consistent with presence of this environment in $Li_2Mn_2O_4$.) Thus, the additional lithium resonances could result from lithium substitution into these sites or from the presence of adjacent manganese vacancies in the lithium local coordination sphere. The most likely sites for lithium substitution are the 16d and 16c sites; indeed, lithium substitution on the 16d site has been confirmed, by diffraction, for the lithium-excess materials.[21] Substitution in these sites, or the presence of a vacancy, will also affect the manganese and lithium ions in the local coordination sphere of the defect. There are two 8a Li^+ ions in the first coordination sphere (in the center of cubes formed by four 16c vacancies and four oxygen atoms (see Figure 10 c)) and a further six in the second coordination sphere. Substitution in the 16d site, or a 16d manganese vacancy, will affect six nearby Li^+ in the 8a site (see Figure 10 b) and a further 8 in the next coordination sphere. Thus, each dopant Li^+ ion will be associated with a number of different resonances. Even if the dopant concentration is small, the numbers of affected lithium cations will be an order of magnitude larger. We tentatively assign the more intense additional resonances at 575−546 ppm to Li^+ cations surrounding the defect.

One explanation for the high-temperature behavior of the lithium spectra and the collapse of the smaller resonances into the main spinel resonance, is that it is due to lithium-ion motion in these systems. If the rate of exchange between different sites becomes greater than the frequency separation of peaks, a motionally averaged single peak is expected.[54] This explanation is not, however, consistent with the very similar ^{6}Li and ^{7}Li spectra at high temperatures: i.e., since the separation between the different resonances is larger for ^{7}Li than for ^{6}Li, in units of frequency, due to the larger gyromagnetic ratio of ^{7}Li, coalescence of the ^{7}Li resonances is expected to occur at a higher temperature than the coalescence of the ^{6}Li resonances. An alternative explanation for the coalescence of the different resonances, and the similar temperature-dependent behavior of the ^{6}Li and ^{7}Li resonances, is that they arise from different trapped electronic states at or near the defect. The e_g orbitals at the manganese ions near the defect will be located at a different energy from those associated with the normal spinel sites, as a result of the slightly different local environment at the manganese site. If the energy of these e_g orbitals is raised by an amount ΔE, then either the electron-hopping process should no longer involve these e_g orbitals ($\Delta E \gg kT$), or the mobile electrons will spend less time in these orbitals (ΔE is approximately equal to or slightly greater than kT). Thus, the lithium ions close to these defects will see adjacent manganese ions with higher oxidation states than those associated with the normal spinel environment. A shift to higher frequency may be expected, on the basis of the Mn(IV) model compounds. A single defect site (vacancy or defect) is associated with a number of nearby distorted manganese environments (e.g., six manganese ions surround a Li^+ in a 16d site defect (Figure 10 b), and as discussed above, a large number of different lithium ions will be affected by the one defect site). At higher temperatures, as

(53) Ammundsen, B.; Rozière, J.; Islam, M. S. *J. Phys. Chem.* **1997**, *101*, 8156.

(54) Stebbins, J. F.; Xu, Z.; Vollath, D. *Solid State Ionics* **1995**, *78*, L1.

the difference in energy between the e_g levels associated with the normal spinel sites and the e_g levels associated with the defect sites decreases in comparison to kT, the e_g orbitals associated with defect sites will become increasingly populated, and the oxidation state of the manganese ions at these sites will decrease. At higher temperatures, the average oxidation state of manganese ions of the defects and the normal sites should converge, and a single resonance is expected for the lithium ions. This mechanism is also consistent with the shift of the main spinel resonance to lower frequencies from LiMn850 (520 ppm) to LiMn550 (498 ppm): increased concentrations on Mn(IV) ions near the defects, or manganese ions with higher average oxidation states, should result in a decrease in the oxidation state for manganese ions in the remainder of the sample. Note, however, that the center of gravity of the resonances ("normal" + those associated with the defects) shifts to higher frequency with lower synthesis temperature. This is in agreement with the results of Goodenough et al. who demonstrated, by titration, that the average Mn oxidation state is increased as the synthesis temperature is decreased.[13] The shift of the center of gravity of the ^{6}Li spectrum of $Li_{1.07}Mn_{1.93}O_4$ to higher frequency, in comparison to the center of gravity of the LiMn850 spectrum, which was synthesized at the same temperature, is consistent with the increased oxidation state of manganese in this lithium-excess compound. Furthermore, the electronic defects are present in the off-stoichiometry spinels, even when the samples are synthesized at high temperatures. The ^{7}Li MAS NMR spectra of a number of commercial samples of lithium−manganate electrode materials, with Li:Mn ratios of greater than 1:2, also contain similar smaller additional resonances that may be assigned to the electronic defects.[55]

The Jahn−Teller Distortion in $LiMn_2O_4$. The changes in line width below room temperature in LiMn650 and LiMn850 are ascribed to the tetragonal Jahn−Teller distortion, which is characteristic of a compound with a (high spin) d^4 electronic configuration. No phase change is observed for LiMn550 and LiMn600, which is consistent with the increase in average manganese oxidation state expected in these materials, and the consequent decrease in the concentration of Mn^{3+} ions.[13] This also explains the suppression of the tetragonal distortion temperature observed for LiMn650, in comparison to LiMn850. The considerable disorder in the LiMn550 and LiMn600 compounds is also likely to be responsible for suppressing the JT distortion in these compounds. The deviation of the ^{6}Li NMR shifts from a simple $1/T$ dependence below room temperature suggests that some changes in the electronic structure of these compounds occur at low temperatures; these changes could be associated with local JT distortions in parts of the sample but may also be related to changes in the populations of the e_g electrons in the manganese ions associated with or near the defects, as discussed in the previous section.

A cubic-to-tetragonal distortion (i.e., from space group $Fd3m$ to $I4_1/amd$) does not create any additional lithium local environments, and a single ^{6}Li NMR resonance is still predicted. This is contrary to the experimental observations where three major resonances (and a shoulder on the "normal" spinel resonance) are observed. Clearly, there is more than one local environment for Li^+, suggesting that there must be at least some partial ordering of the e_g electron on the manganese site, in the time scale of the NMR experiment.

Ordering schemes of the Mn^{3+} and Mn^{4+} ions have been discussed by Sugiyama et al. in order to rationalize the abrupt increase in line width that occurs below the antiferromagnetic ordering temperature (at 40 K, in their sample).[38] Two models were considered; one involved random distributions of Mn^{3+} and Mn^{4+} ions on the 16d sites where each lithium ion was assumed to coordinate to the same number of Mn^{3+} and Mn^{4+} ions in order to maintain charge neutrality. The second model involved short-range ordering of Mn^{3+} and Mn^{4+} ions: the Mn^{3+} ions occupied sites at $x = {}^1/_8$ and $^5/_8$ while the Mn^{4+} ions occupied sites at $x = {}^3/_8$ and $^7/_8$, in analogy with the ordering seen in Fe_3O_4.[56] Both of these models gave rise to a distribution of local fields that were consistent with the observed ^{7}Li data, and the presence of long-range ordering could not be definitively established. In addition, these authors examined the small changes in the susceptibility χ that occurred around the cubic-to-tetragonal phase transition, to try and detect any evidence for any ordering. A very small change in the slope of $1/\chi$ vs T was detected, which they suggested was indicative of local JT distortions.

To rationalize our ^{6}Li MAS NMR results, a model where the Mn^{3+} and Mn^{4+} ions are randomly distributed over the lattice is considered initially. Assuming that the e_g electrons are now (at least partially) localized in the d_{z^2} orbitals of the manganese ions below the transition temperature (as expected for a JT system with unit cell parameters c and a of $c > a$), then there are a number of possible lithium local environments: $Li(OMn^{3+})_{12-x}(OMn^{4+})_x$. Too many resonances are predicted with this ordering scheme, and we can rule this out. Even if we need only consider the effect on the ^{6}Li shift of the four manganese ions that are coordinated via their d_{z^2} orbitals to the oxygen atoms adjacent to Li^+, five resonances are still predicted, with intensities (1:4:6:4:1) that do not correspond to the experimentally observed intensities. Other ordering schemes can be also envisaged; the scheme discussed by Sugiyama et al.[38] does not create any new lithium environments and each ion is surrounded by 6 Mn^{3+} and 6 Mn^{4+} ions. If, however, the Mn^{3+} ions occupy sites at $x = {}^3/_8$ and $^5/_8$ while the Mn^{4+} ions occupy sites at $x = {}^1/_8$ and $^7/_8$, three different local environments are created: $Li(OMn^{3+})_4(OMn^{4+})_8$, $Li(OMn^{3+})_6(OMn^{4+})_6$, and $Li(OMn^{3+})_8(OMn^{4+})_4$, with concentrations 1:2:1, respectively, which should result in three different resonances. Analogous ordering schemes along z are also possible. The experimentally observed intensities for the main resonances are not, however, a simple 1:1:2, the resonance at higher frequency (688 ppm) being approximately 70% of the intensity of the resonance 633 ppm at −40 °C for LiMn850. Thus, we can conclude that the charge localization does not appear to be random or to include any of these simpler arrangements discussed above.

Conclusions

A discrete ^{6}Li resonance (at 1980 ppm) has been observed for lithium substitution into the (octahedral) manganese site of the lithium manganese spinel $Li_4Mn_5O_{12}$, demonstrating that ^{6}Li MAS NMR may be used to probe lithium-ion substitution on the different lattice sites of the spinel structure. This resonance and the resonances observed for other Mn(IV) compounds have been used to rationalize the direction and magnitude of the different hyperfine shifts: The largest shift is observed for a Li−O−Mn bond angle of 90°, which is consistent with either a direct interaction of the t_{2g} and lithium 2s orbitals, or a π interaction involving the intervening 2p orbital and the manganese t_{2g} orbitals. Much smaller hyperfine shifts are observed for Mn(III) compounds, while the shifts for the

(55) Lee, Y. J.; Grey, C. P., unpublished results.

(56) Verway, E. J. W.; Haayman, P. W. *Physica* **1941**, *8*, 979.

$LiMn_2O_4$ spinels, with average manganese oxidation state of 3.5, lie between the Mn(III) and Mn(IV) hyperfine shifts.

^{6}Li MAS NMR spectra of spinels with the nominal composition $LiMn_2O_4$ are extremely sensitive to small amounts of disorder, and to heterogeneity in the electronic structure of the manganese ions, throughout the sample. A clear relationship between synthesis conditions and lithium local order is observed, the spinels synthesized at lower temperature showing greater Li^+ disorder. Electronic defects, which are associated with manganese ions in higher oxidation states, are trapped in the spinel lattice as a result of this disorder. These electronic defects are also present in lithium-excess spinel materials such as $Li_{1.07}Mn_{1.93}O_4$ and in commercial materials which, typically, have Li:Mn ratios of greater than 0.5. We are currently in the process of investigating the effect of these defects on the cycling behavior of these materials when used as electrodes in lithium cells.

A number of different lithium local environments are observed for the tetragonal spinel phases, as a result of the static JT distortion that occurs at low temperatures for the more ordered compounds. This indicates that the e_g electrons are, at least, partially ordered in the time scale of the NMR experiment. This ordering has not previously been definitively demonstrated with any other analytical technique or with wide-line NMR. The lack of a JT distortion in the compounds synthesized at lower temperatures is not only a function of manganese oxidation state, as has been previously suggested, but is alsolikely be related to the disorder and defects present in these samples.

In conclusion, ^{6}Li MAS NMR has been shown to be extremely sensitive to cationic disorder, the presence of defects, Li:Mn ratio, and changes in manganese oxidation state, all factors that have all been implicated in the success of certain lithium−spinel compositions and samples as electrode materials in lithium batteries. The improved understanding of the lithium spectra of these materials that has resulted from this study will help in the interpretation of NMR spectra of a greater range of lithium-containing manganates and, in particular, the spectra of lithium manganate electrode materials following lithium discharging and charging processes. Finally, these NMR studies should lead to an improved understanding of the local atomic and electronic structures of these materials following synthesis and during the charging/discharging processes.

Acknowledgment. This research was supported via a grant from the National Science Foundation to purchase a solid state NMR spectrometer (CHE-9405436) and through the National Young Investigator Program (DMR-9458017). Drs. Sanjeev Mukerjee and James McBreen are thanked for helpful discussions. Help from Professor Peter Stephens with the experiments performed at the NSLS is gratefully acknowledged.

JA9817794